Journal of Power Sources 196 (2011) 8104–8109

Contents lists available at ScienceDirect

Journal of Power Sources

journal homepage: www.elsevier.com/locate/jpowsour

Improved electrochemical activity of $LiMnPO_4$ by high-energy ball-milling

Jiangfeng Ni[a,*], Yoshiteru Kawabe[b], Masanori Morishita[b], Masaharu Watada[b], Tetsuo Sakai[a,*]

[a] National Institute of Advanced Industrial Science and Technology, 1-8-31 Midorigaoka, Ikeda, Osaka 563-8577, Japan
[b] GS Yuasa International Ltd, Nishinosho, Kisshoin, Minami-ku, Kyoto 601-8520, Japan

ARTICLE INFO

Article history:
Received 26 January 2011
Received in revised form 21 April 2011
Accepted 16 May 2011
Available online 27 May 2011

Keywords:
Lithium ion battery
Lithium manganese phosphate
High-energy ball-milling
Electrochemical activity
Synchrotron radiation

ABSTRACT

Olivine lithium manganese phosphate ($LiMnPO_4$) becomes research focus because of its high energy density and improved thermal stability. However, its application in lithium ion batteries suffers severely from poor electrochemical activity due to low conductivity and structural instability upon the charge and discharge process. By applying a high-energy ball-milling method we succeed in improving the capacity delivery and rate capability. $LiMnPO_4$ materials ball-milled without or with acetylene black are able to deliver a high capacity of 135 and 127 mAh g^{-1}, respectively, more than 50% greater than the pristine one. Particularly, the latter also shows an improved discharge plateau and stable cyclability. High-energy synchrotron radiation X-ray diffraction (XRD), scanning electron microscopy (SEM), Raman spectroscopy, laser particle analysis, and galvanostatic charge and discharge are employed to understand the effect of ball-milling on the $LiMnPO_4$ material.

1. Introduction

The boom demand for high energy and power relies heavily on the current secondary battery systems, particularly on Li-ion batteries [1,2]. Although the Li-ion batteries have been widely applied in most portable electronic devices such as laptops, digital cameras and mobile phones, their enlargement of application in power tools and automotive industry is severely hindered due to the intrinsic safety limitation of currently major cathode material $LiCoO_2$. To address this issue, many cathode materials based on XO_m (PO_4, SiO_4, BO_3, etc.) polyanion structures have been explored due to the decent redox potential and improved safety [3–5]. The strong covalent X–O bond of the XO_m polyanions not only enhances the M^{2+}/M^{3+} redox potential through an inductive effect, but also prevents the O atoms from releasing even in abused condition. In particular, the olivine $LiFePO_4$ material has received a great deal of attention because of good electrochemical property, high thermal stability, low raw material cost, and environmental benignity [6,7].

However, $LiFePO_4$ shows a relatively low energy density because of a lower operating voltage of 3.4 V vs. Li^+/Li compared with 3.9 V of $LiCoO_2$ and 4.1 V of $LiMn_2O_4$. This poor energy density indicates more battery modules are needed, which is not so easy to meet in the power systems. Therefore, a cathode material with a high operating voltage is highly desirable. $LiMnPO_4$ seems to be an ideal choice because it possesses a large theoretical capacity (170 mAh g^{-1}), a good thermal stability, and a high operating voltage of 4.1 V vs. Li^+/Li, which is comparable with currently commercial materials [3,8].

Due to poor electrochemical behavior, however, the application of $LiMnPO_4$ in power batteries still faces a great challenge. Two major factors are believed to account for this. One is the extremely low electronic and ionic conductivity, and the other is the structural instability upon the electrochemical process. Over last decades, the poor conductivity issue in olivine materials has been significantly addressed by carbon coating or ion doping [9,10]. However, the structural issue has not been well taken care of [11,12]. It is fairly well known that the charged $LiMn^{II}PO_4$ phase undergoes a severe lattice deformation due to the asymmetric electronic configuration of Mn^{3+} ions ($3d^4$ ($t_{2g}^3 e_g^1$)) [13,14]. The Jahn–Teller deformation as well as the large lattice misfit between $LiMnPO_4$ and $MnPO_4$ phases destroys the integrity of lattice, thus leading to a low electrochemical activity. As a consequence, the capacity delivery of $LiMnPO_4$ is quite low in early reports [15–17]. For instance, Delacourt et al. reported a capacity of 70 mAh g^{-1} for $LiMnPO_4$ prepared via an aqueous precipitation route [15].

Later, it is demonstrated that the performance of $LiMnPO_4$ can be improved when carefully controlling its size, morphology and texture [18–20]. For instance, Kwon et al. shows that $LiMnPO_4$ could deliver a capacity of 134 mAh g^{-1} at 0.1 C when the particle size decreasing to 140 nm [19]. More recently, Wang et al. adopted a polyol synthesis approach to prepare platelet-like $LiMnPO_4$ nanostructures with ultrathin [020] crystalline plane (~20 nm), which could deliver a high capacity of 141 mAh g^{-1} [21].

* Corresponding authors. Tel.: +81 72 751 9611; fax: +81 72 751 9623.
E-mail addresses: jfengni@gmail.com (J. Ni), sakai-tetsuo@aist.go.jp (T. Sakai).

0378-7753/$ – see front matter © 2011 Elsevier B.V. All rights reserved.
doi:10.1016/j.jpowsour.2011.05.038

After being further ball-milled with carbon black, the obtained $LiMnPO_4$–C composite is comprised of spherical particles with size in the range of 25–30 nm. Such nanocomposite exhibits a stable capacity up to 145 mAh g^{-1} in the potential range of 2.7–4.4 V [22]. This report represents the strategy to improve the activity of $LiMnPO_4$ towards lithium: efficient carbon coating and synthesis of nanoparticle (generally less than 50 nm). The former provides good electrical conduct between particles and current collector, while the latter enhances Li ion diffusion as well as structural flexibility towards lattice deformation [23]. Inspired by this work, many recent works follow such a fashion [24,25]. However, the nanoscale particles coupled with a heavy carbon loading (≥25 wt.%) decrease the volumetric energy density and raise the difficulty of material processing. Therefore, it may not be appealing for practical application.

Another strategy to improve the electrochemical activity of $LiMnPO_4$ is to dope exotic ions, as widely utilized in $LiFePO_4$ [26,27]. It is proposed that doping in $LiMnPO_4$ may modify the electronic conductivity and the structural compatibility upon the electrochemical process, thus leading to a high activity [28,29]. However, the mechanism for doping is not clear yet, as it is discovered that some ions (Mg^{2+}, Fe^{2+}, Ni^{2+}, and Cu^{2+}) show a positive effect on the electrochemical performance of $LiMnPO_4$, whereas other ions (Zn^{2+} and Ca^{2+}) show a negative one [28–32].

So far, it is still a challenge to prepare high-performance $LiMnPO_4$ material via a facile method. Herein, we introduce a simple post treatment, i.e., high-energy ball-milling, to increase the electrochemical activity of $LiMnPO_4$. The high-energy ball-milling, also known as the mechanochemical method, brings intensive effects on the structure, morphology, and size distribution of the electrode materials, thereby modifying their electrochemical behavior [33,34]. In this work, we report the effects of high-energy ball-milling upon the crystalline property, size, and morphology of $LiMnPO_4$. The effects were further correlated with the electrochemical activity to understand the mechanism.

2. Experimental

The $LiMnPO_4$ material was prepared via a ceramic route with starting materials of Li_2CO_3 (99%, Wako), $MnC_2O_4{\cdot}2H_2O$ (98%, Wako) and $NH_4H_2PO_4$ (99%, Wako). Stoichiometric amount of raw materials was weighed and mixed by mortar and pestle. A certain amount of sucrose as a conductive precursor was added, which was expected to generate 2 wt.% carbon coating in the final product. The mixture was firstly decomposed at 300 °C for 2 h, and then heated at 650 °C for 5 h in continuous Ar flow to obtain the carbon-coated $LiMnPO_4$ (labeled as pristine). The $LiMnPO_4$ was further treated by a high-energy ball-milling process. Typically, 1 g pristine $LiMnPO_4$ material and 100 g ZrO_2 balls (φ 4 mm) were loaded into a Teflon-lined stainless steel vessel, and sealed in Argon filled glove box. Then the vessel was fixed on a high-speed planetary mill (High G, Kurimoto) and operated at a speed of 500 rpm with an input power of 3.7 kW. The milling time lasted for 2 h with interval of 30 min for every half hour. After treatment, the powder was separated from ZrO_2 balls by sieving and collected for characterization. Two ball-milling products, without or with acetylene black (8 wt.%), were produced. The final products are accordingly labeled as HG1 and HG2.

X-ray diffraction (XRD) measurement was conducted at the BL19B2 beam line of the synchrotron radiation facility SPring-8, Japan, as reported elsewhere [35]. A large Debye–Scherrer camera was used to detect the fine diffraction patterns, and the wavelength was calibrated to be λ = 0.70 Å by using CeO_2 as a standard. A glass capillary (φ = 0.3 mm) was used to load $LiMnPO_4$ powder and sealed in an Ar filled glove box. The structural analysis was performed with the Rietveld method on the program Rietan-2000 [36]. Scanning electron microscopy (SEM) was carried out on a JEOL JSM-6390 microscope. Raman spectroscopy was performed on a RMP-320 (Jasco) spectrometer with Ar laser of 50 mW at 532 cm^{-1}. Particle size distribution was analyzed by a laser particle analyzer (Mastersizer 2000, Malven).

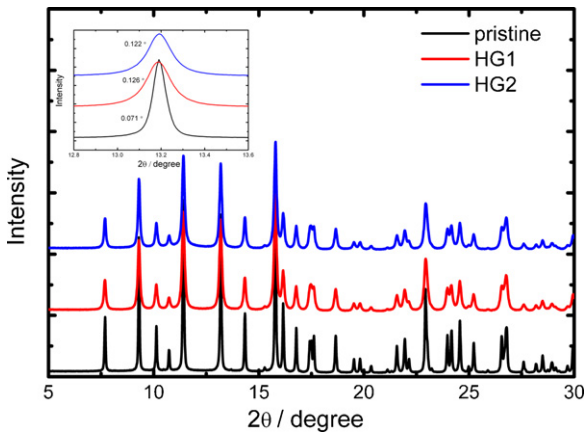

Fig. 1. XRD patterns of the pristine and ball-milled $LiMnPO_4$ materials.

The electrochemical tests were carried out on a 2032 coin cell. The cathode composite consists of 80 wt.% $LiMnPO_4$, 10 wt.% acetylene black (inclusive of that over the ball-milling process), and 10 wt.% polyvinylidene fluorine, with a typical material loading of 5 mg cm^{-2}. The 2032 coin cells were assembled in a dry room with a dew point below −60 °C. The anode is Li foil, and the electrolyte is 1 mol L^{-1} $LiPF_6$ in ethylene carbonate/dimethyl carbonate (EC/DMC) (1:1 by volume). The cells were measured on a Battery Lab System program-controlled test system (Keisokuki Center) in the voltage range of 2.2–4.5 V.

3. Results and discussion

The XRD patterns of as-prepared three $LiMnPO_4$ materials (pristine, HG1, and HG2) are presented in Fig. 1. All the patterns show well resolved diffraction peaks indexed to olivine $LiMnPO_4$ (JCPDS no. 74-0375) without any impurities. This indicates that the $LiMnPO_4$ material can be readily synthesized by this ceramic route, and that the structure remains after the post high-energy ball-milling process. A zoom look (inset in Fig. 1) reveals that the peak intensities decline and the peaks become broad for the ball-milled sample, suggesting that both the crystallinity and crystalline size are decreased [33,34]. This phenomenon would be more pronounced when using Cu Kα diffraction (not shown). By using the Scherrer formula $D = 0.9\lambda/\beta\cos\theta$, where λ is the X-ray wavelength, β the full width at half maximum (FWHM), θ the Bragg angle, the average crystalline size D along [0 2 0] direction can be calculated to be 48, 27, and 28 nm for pristine, HG1 and HG2 materials, respectively. Since Li^+ ion diffusion in $LiMnPO_4$ occurs along the one-dimensional direction paralleling to the b-axis, such a decrease in crystalline size would facilitate Li ion diffusion within particles.

The structural refinement was performed on the synchrotron XRD data of $LiMnPO_4$ materials. Table 1 summarizes R factors and some lattice parameters, and Fig. 2 presents the refinement result of the typical pristine $LiMnPO_4$. All refinements give satisfactory values of R_{wp}, R_p, and S, indicating that the structural analysis is reliable. The pristine $LiMnPO_4$ has the lattice parameters of a = 10.444(1) Å, b = 6.102(1) Å, c = 4.744(1) Å, and V = 302.35 $Å^3$, agreeing well with the previous reports [3,15,30]. The ball-milled materials, however, show a slight increase in lattice parameters, with an overall 0.3% expansion in the unit cell volume. A bit of

Table 1
The *R* factors and structural parameters of $LiMnPO_4$ materials.

Sample	*a* (Å)	*b* (Å)	*c* (Å)	*V* (Å^3)	Li–O_1 (Å)	Li–O_2 (Å)	Li–O_3 (Å)	R_{wp} (%)	R_p (%)	*S*
Pristine	10.444(1)	6.102(1)	4.744(1)	302.35	2.241	2.103	2.159	4.00	2.98	1.05
HG1	10.454(4)	6.108(2)	4.748(2)	303.16	2.256	2.106	2.152	4.50	3.40	1.19
HG2	10.455(6)	6.108(3)	4.747(2)	303.15	2.251	2.105	2.149	4.32	3.26	1.13

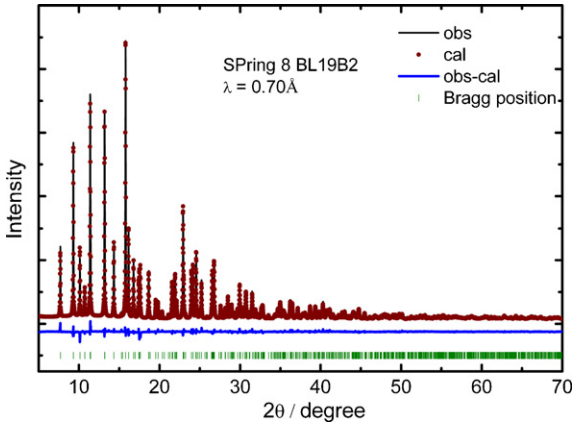

Fig. 2. Rietveld refinement results of the pristine $LiMnPO_4$ material.

expansion in LiO_6 octahedral is also confirmed. Such expansion reflects the strong interaction between material particles and ZrO_2 balls [33], and may benefit the Li^+ ion diffusion [27]. In addition, lattice defects such as the voids and cracks and amorphous state may be generated by the ball-milling treatment [33,34], which can accommodate the lattice stress and strain induced by Jahn–Teller deformation. Consequently, an improved electrochemical activity could be anticipated.

SEM images of the $LiMnPO_4$ materials are illustrated in Fig. 3a–c. The pristine material is composed of many submicron grains and a few agglomerates up to several microns. In contrast, the ball-milled materials are dominated by fine particles, which are the fragments of large particles. This scenario is particularly impressive in HG1 material, as the interaction between ZrO_2 balls and $LiMnPO_4$ particles proceeded without buffering of acetylene black. It is worthy of noting that some large agglomerates are also observed in the SEM image of HG1, which may be due to the recombination of the resultant small $LiMnPO_4$ fragments driven by the large surface energy. Fig. 3d shows the Raman spectra of three $LiMnPO_4$ materials in which only two sets of bands centered at 1345 and 1590 cm^{-1} are observed. These bands are due to the D band and G band of carbon, respectively [35]. The other bands associated with PO_4^{3-} group, however, are not visible, probably being masked by the strong scattering signal of carbon.

The materials were further characterized by laser particle analysis. Fig. 4 represents their volume size distributions. The ball-milled

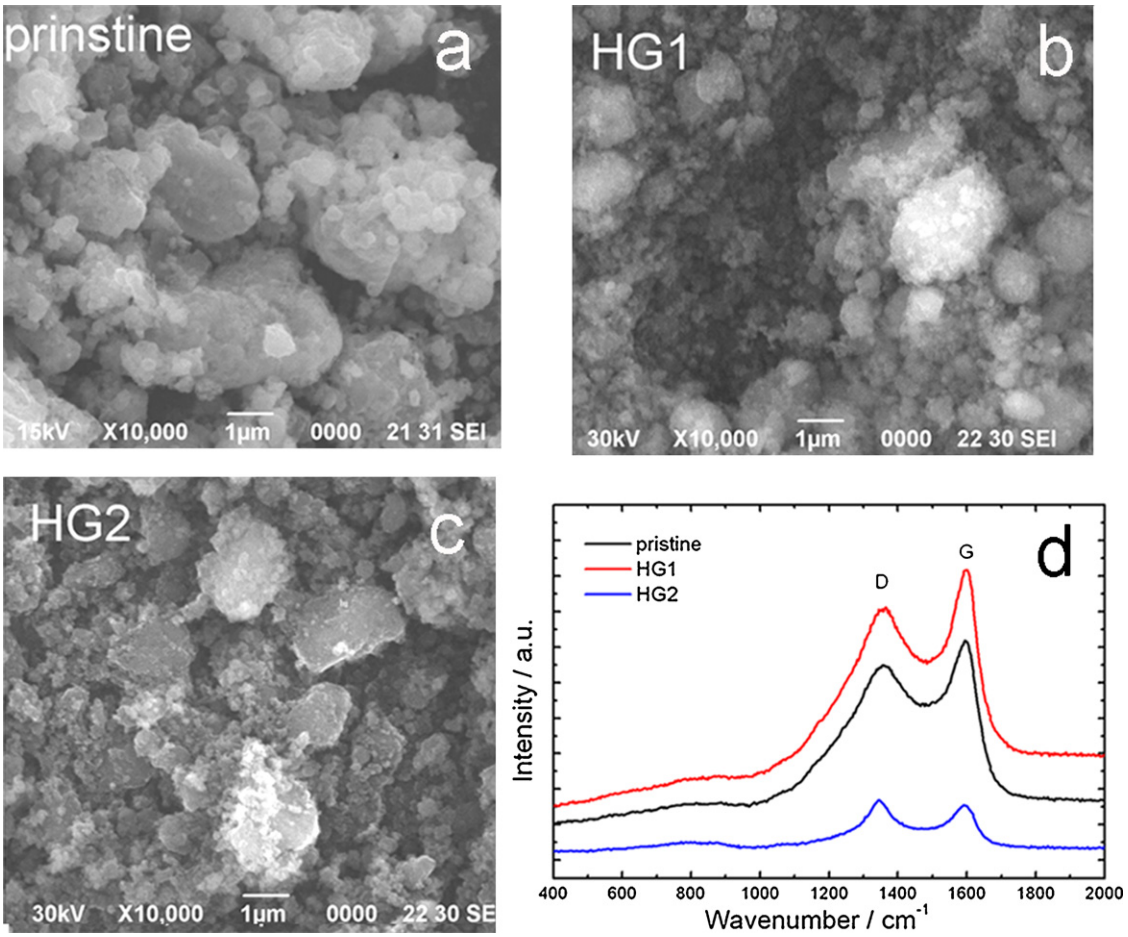

Fig. 3. SEM images (a–c) and Raman spectra (d) of the pristine and ball-milled $LiMnPO_4$ materials.

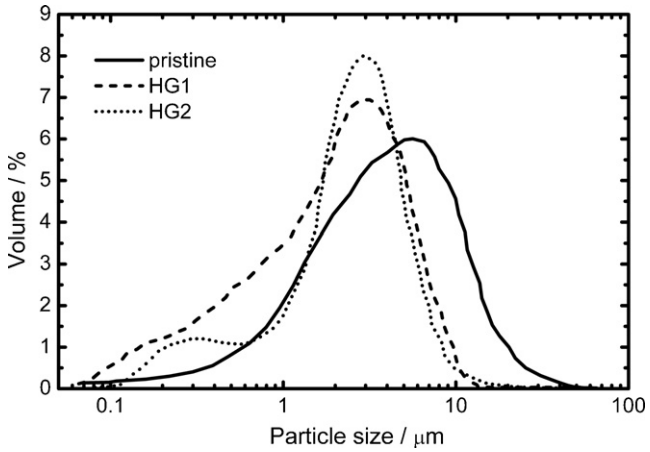

Fig. 4. Volumetric particle size distribution of the $LiMnPO_4$ materials.

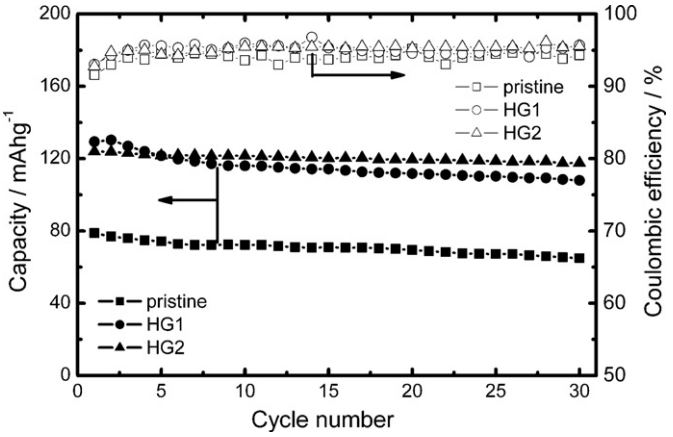

Fig. 6. Discharge capacity and coulombic efficiency of the three $LiMnPO_4$ electrodes at 0.1 C and 30 °C as a function of cycle number.

materials clearly show a decreased particle size compared with the pristine one. The fraction of coarse particles (>20 μm) in the profile of the pristine material also disappear in both HG1 and HG2. In addition, HG1 shows a broad distribution below 1 μm, indicating the existence of fine particles, whereas HG2 shows a side peak around 0.2 μm, which may be due to added acetylene black.

The electrochemical activity was investigated using the Li coin cells. Fig. 5 compares their initial charge and discharge profiles at 0.05 C (1 C = 150 mA g^{-1}) at 30 °C. In the range of 2.2–4.5 V, the pristine $LiMnPO_4$ material only delivers a capacity of 83 mAh g^{-1}, whereas HG1 and HG2 deliver 135 mAh g^{-1} and 127 mAh g^{-1}, respectively, which are 63% and 53% greater than the pristine. The enhanced capacity may be attributed to the improved Li diffusion kinetics and the better tolerant ability towards lattice stress. The former is attributed to decreased particle size, while the latter may be related to defects and partial amorphous state. Note that the capacity is somewhat lower than that of Martha et al. [22] and Oh et al. [25], due to the low carbon loading in our case (12 wt.% compared with 30 wt.% or more). However, our materials may deliver a higher energy density. To address this issue in detail, we compare the volumetric energy density of two $LiMnPO_4$ electrodes by a simple calculation: electrode (1) 78 wt.% $LiMnPO_4$ + 12 wt.% C + 10 wt.% binder and electrode (2) 60 wt.% $LiMnPO_4$ + 30 wt.% C + 10 wt.% binder. The compacted densities are 1.8 and 1.4 g cm^3 for electrode (1) and (2), respectively. Assuming their reversible capacity are 125 and 155 mAh g^{-1}, we can calculate their volumetric energy densities to be 176 and 130 mAh cm^3, respectively. This clearly shows that our material is more favorable to high energy density.

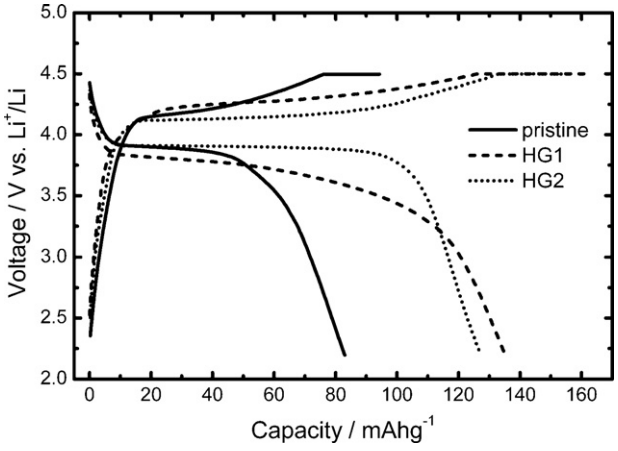

Fig. 5. The initial charge and discharge profiles of the pristine and ball-milled $LiMnPO_4$ electrodes at 0.05 C and 30 °C.

It is worth mentioning that HG1 exhibits a large polarization over the charge and discharge despite the high capacity. The polarization refers to the poor electrical conduction as the carbon coating layer in HG1 may be severely destroyed by ball-milling, whereas this damage is minimized in HG2 where acetylene black provides a buffer. Further electrochemical impedance spectroscopy results (not shown) confirm the hypothesis.

The cycling performance of the $LiMnPO_4$ electrodes at 0.1 C rate and 30 °C is shown in Fig. 6. The cells were fully charged and discharged at 0.05 C for three cycles before the cycling test. The pristine $LiMnPO_4$ exhibits a low capacity retention of 82% after 30 cycles. Similarly, HG1 shows appreciable capacity decay over the cycles despite its high initial capacity of 130 mAh g^{-1}. It falls down to 108 mAh g^{-1} at the 30 cycles, possibly due to its poor conductivity. This is because some particles in HG1 electrode may easily lose electrical connection with current collector driven by large volume variation upon cycles. In contrast, HG2 shows a marked improved retention up to 95%, delivering the highest capacity of 118 mAh g^{-1} among the three samples at the 30th cycles. The enhanced structural integrity due to lattice defects and the intact conducting layer are believed to account for such a high cycling stability. The high coulombic efficiencies (>95%) of the milled materials verify that their electrochemical process is reversible, as shown in Fig. 6.

To evaluate the power ability of these $LiMnPO_4$ materials, rate discharge experiments were further carried out. The coin cells were charged it at a constant current of 0.1 C to 4.5 V followed by holding at 4.5 V until current decaying to 0.02 C, and then discharged to 2.2 V at various rates. The rate discharge profiles of the three $LiMnPO_4$ samples are presented in Fig. 7. As anticipated, enhanced rate capabilities are observed in all rates for both ball-milled $LiMnPO_4$ samples compared with the pristine one. When the current rate increases from 0.05 C to 1 C, the capacity of the pristine $LiMnPO_4$ drops from 81 mAh g^{-1} to 50 mAh g^{-1}. Meanwhile, the capacities of HG1 are 134 mAh g^{-1} and 96 mAh g^{-1} at 0.05 C and 1 C, respectively. HG2 shows a similar rate behavior to HG1, 127 mAh g^{-1} at 0.05 C, 123 mAh g^{-1} at 0.1 C, and 99 mAh g^{-1} at 1 C. It is also seen that HG2 displays a flat discharge plateau at 0.05–0.4 C rate, in vast contrast to the sloping curves of HG1 even at 0.05 C. This suggests that the acetylene black protects the coating carbon layer while does not counteract the effect of ball-milling. Therefore, ball-milling with conductive carbon serves as a better modification approach for

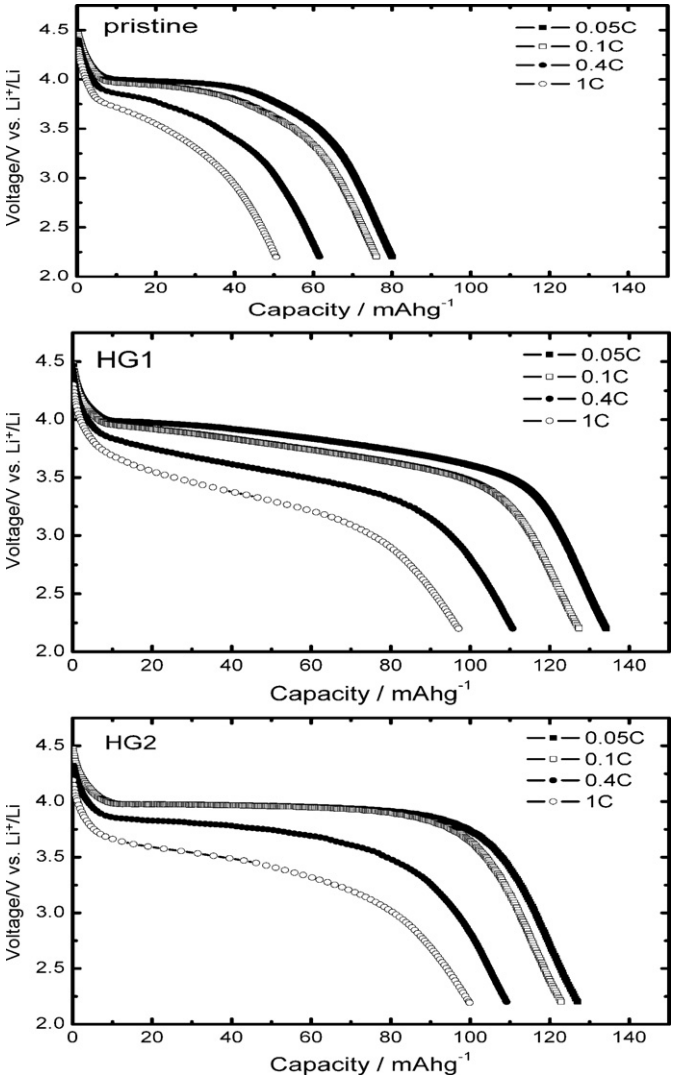

Fig. 7. Rate discharge capability of the three $LiMnPO_4$ electrodes at 30 °C. The cells were charged at a CC-CV protocol, i.e., first charged at a constant current of 0.1 C to 4.5 V followed by holding at 4.5 V until current decaying to 0.02 C.

$LiMnPO_4$. A similar conclusion was also drawn by Rabanal et al. [34].

It is interesting to note that the HG1 material delivers an even higher capacity than HG2 at the low rates despite the large polarization, which is not fully clear currently. One possible reason is that HG1 may possess more defects and amorphous state due to the direct interaction between material and ZrO_2 balls, which provides a better tolerant ability to internal stress and strain. At low rates, the limitation of conductivity is not critical, while the relaxation of lattice strain would be the key fact influencing the electrochemical activity. Investigation of lattice defects by high resolution TEM is currently under way to gain an insight into this issue.

It is well known Jahn–Teller distortion is one of the main reasons that lead to a poor cycling behavior of manganese based materials. Therefore, the $LiMnPO_4$ electrodes were also measured at 55 °C to examine the possible effect of Jahn–Teller distortion. Fig. 8 depicts the cyclability of the typical sample HG2 at 55 °C. The material, however, exhibits a good cyclabity with only ~2.5 mAh g^{-1} lost after 40 cycles, equal to a capacity fading of 0.05% per cycle. Hereby it is manifest that the Jahn–Teller distortion has little impact on the ball-milled $LiMnPO_4$ material.

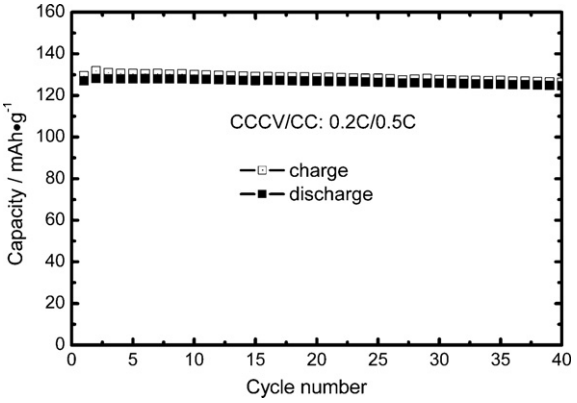

Fig. 8. Discharge capacity of HG2 electrode at 55 °C as a function of cycle number. Charge rate: 0,2 C, discharge rate: 0.5 C.

4. Conclusion

In summary, a simple high-energy ball-milling approach was proposed to improve the electrochemical activity of $LiMnPO_4$. The $LiMnPO_4$ sample ball-milled with 8 wt.% acetylene black shows an increased capacity, stable cycling behavior, and good rate capability. On the other hand, the ball-milled sample without acetylene black shows a high capacity of 135 mAh g^{-1} but an appreciable capacity fading over cycling. The improved electrochemical activity may be attributed to enhanced kinetics and structure integrity, which are related to the decreased particle size, expanded unit cell volume, and crystal defects. It is believed that the activity of $LiMnPO_4$ can be further improved given that the ball-milling parameters like time, material/ball ratio, and conductive additive are optimized. Although it may be not as effective as some soft-chemical methods that can elaborately tailor the physicochemical nature of final products, the mechanochemical method is, due to simplicity and easy operation, still attractive and in principle applicable to other electrode materials with poor structural integrity.

References

[1] M.S. Whittingham, Chem. Rev. 104 (2004) 4271.
[2] B. Scrosati, J. Garche, J. Power Sources 195 (2010) 2419.
[3] A.K. Padhi, K.S. Nanjundaswamy, J.B. Goodenough, J. Electrochem. Soc. 144 (1997) 1188.
[4] A. Nyten, A. Aboumrane, M. Armand, T. Gustafson, J.O. Thomas, Electrochem. Commun. 7 (2005) 156.
[5] V. Legagneur, Y. An, A. Mosbah, R. Portal, A. Le Gal La Salle, A. Verbaere, D. Guyomard, Y. Piffard, Solid State Ionics 139 (2001) 37.
[6] Y.-H. Huang, J.B. Goodenough, Chem. Mater. 20 (2008) 7237.
[7] M. Yao, K. Okuno, T. Iwaki, M. Kato, S. Tanase, K. Emura, T. Sakai, J. Power Sources 173 (2007) 545.
[8] S. Okada, S. Sawa, M. Egashira, J.-I. Yamaki, M. Tabuchi, H. Kageyama, T. Konishi, A. Yoshino, J. Power Sources 97–98 (2001) 430.
[9] Y.G. Wang, Y.R. Wang, E. Hosono, K.X. Wang, H.S. Zhou, Angew. Chem. Int. Ed. 47 (2008) 1.
[10] X.-L. Wu, L.-Y. Jiang, F.F. Cao, Y.-G. Guo, L.-J. Wan, Adv. Mater. 21 (2009) 2710.
[11] A. Yamada, M. Hosoya, S.-C. Chung, Y. Kudo, K. Hinokuma, K.-Y. Liu, Y. Nishi, J. Power Sources 119–121 (2003) 232.
[12] Z.X. Nie, C.Y. Ouyang, J.Z. Chen, Z.Y. Zhong, Y.L. Du, D.S. Liu, S.Q. Shi, M.S. Lei, Solid State Commun. 150 (2010) 40.
[13] Y.G. Xia, Q. Zhang, H.Y. Wang, H. Nakamura, H. Noguchi, M. Yoshio, Electrochim. Acta 52 (2007) 4708.
[14] G. Amatuci, J.-M. Tarascon, J. Electrochem. Soc. 149 (2002) K31.
[15] C. Delacourt, P. Poizot, M. Morcrette, J.-M. Tarascon, C. Masqulier, Chem. Mater. 19 (2004) 93.
[16] C. Delacourt, L. Laffont, R. Bouchet, C. Wurm, J.-B. Leriche, M. Morcrette, J.-M. Tarascon, C. Masqulier, J. Electrochem. Soc. 152 (2005) A913.
[17] H. Fang, L. Li, G. Li, Chem. Lett. 36 (2007) 436.
[18] L. Wang, F. Zhou, G. Ceder, Electrochem. Solid-State Lett. 11 (2008) A94.
[19] N.-H. Kwon, T. Drézen, I. Exnar, I. Teerlinck, M. Isono, M. Graetzel, Electrochem. Solid-State Lett. 9 (2006) A277.
[20] T. Drézen, N.-H. Kwon, P. Bowen, I. Teerlinck, M. Isono, I. Exnar, J. Power Sources 174 (2007) 949.

[21] D. Wang, H. Buqa, M. Crouzet, G. Deghenghi, T. Drézen, I. Exnar, N.-H. Kwon, J.H. Miners, L. Poletto, M. Grätzel, J. Power Sources 189 (2009) 624.
[22] S.K. Martha, B. Markovsky, J. Grinblat, Y. Gofer, O. Haik, E. Zinigrad, D. Aurbach, T. Drézen, D. Wang, G. Deghenghi, I. Exnar, J. Electrochem. Soc. 157 (2009) A541.
[23] Y.-G. Guo, J.-S. Hu, L.-J. Wan, Adv. Mater. 20 (2008) 2878.
[24] Z. Bakenov, I. Taniguchi, Electrochem. Commun. 12 (2010) 75.
[25] S.-M. Oh, S.-W. Oh, C.-S. Yoon, B. Scrosati, K. Amine, Y.-K. Sun, Adv. Funct. Mater. 20 (2010) 3260.
[26] S.Y. Chung, J.T. Bloking, Y.M. Chiang, Nat. Mater. 1 (2002) 123.
[27] H. Liu, Q. Cao, L.J. Fu, C. Li, Y.P. Wu, H.Q. Wu, Electrochem. Commun. 8 (2006) 1553.
[28] D. Wang, C. Ouyang, T. Drézen, I. Exnar, A. Kay, N.-H. Kwon, P. Gouerec, J.H. Miners, M. Wang, M. Grätzel, J. Electrochem. Soc. 157 (2010) A225.
[29] G. Chen, J.D. Wilcox, T.J. Richardson, Electrochem. Solid-State Lett. 11 (2008) A190.
[30] T. Shiratsuchi, S. Okada, T. Doi, J.-I. Yamaki, Electrochim. Acta 54 (2009) 3145.
[31] J.-W. Lee, M.-S. Park, B. Anass, J.-H. Park, M.-S. Paik, S.-G. Doo, Electrochim. Acta 55 (2010) 4162.
[32] J. Molenda, W. Ojczyk, J. Marzec, J. Power Sources 174 (2007) 689.
[33] L.J. Ning, Y.P. Wu, S.B. Fang, E. Rahm., R. Holze, J. Power Sources 133 (2004) 229.
[34] M.E. Rabanal, M.C. Gutierrez, F. Garcia-Alvarado, E.C. Gonzalo, M.E.A. Dompablo, J. Power Sources 160 (2006) 523.
[35] J. Ni, M. Morishita, K. Yoshiteru, M. Watada, N. Takeichi, T. Sakai, J. Power Sources 195 (2010) 2877.
[36] F. Izumi, T. Ikeda, Mater. Sci. Forum (2000) 321.